Applied Catalysis B: Environmental 145 (2014) 101–107

Contents lists available at ScienceDirect

Applied Catalysis B: Environmental

journal homepage: www.elsevier.com/locate/apcatb

Effect of support-active phase interactions on the catalyst activity and selectivity in deoxygenation of triglycerides

David Kubička[a,*], Jan Horáček[a], Michal Setnička[b], Roman Bulánek[b], Arnošt Zukal[c], Iva Kubičková[a]

[a] Research Institute of Inorganic Chemistry, RENTECH-UniCRE, Chempark Litvínov, Záluží – Litvínov, 436 70, Czech Republic
[b] Department of Physical Chemistry, Faculty of Chemical Technology, University of Pardubice, Studentská 573, 532 10 Pardubice, Czech Republic
[c] J. Heyrovský Institute of Physical Chemistry, Academy of Sciences of the Czech Republic, v.v.i., Dolejškova 3, 182 23 Prague, Czech Republic

ARTICLE INFO

Article history:
Received 14 October 2012
Received in revised form
25 December 2012
Accepted 11 January 2013
Available online 18 January 2013

Keywords:
Deoxygenation
Vegetable oils
Effect of support
Supported NiMo catalysts

ABSTRACT

Three industrially important supports, SiO_2, TiO_2 and Al_2O_3, were used for preparation of NiMo catalysts (3.3 wt.% Ni and 15.0 wt.% Mo) and used in deoxygenation of rapeseed oil in presence of hydrogen (3.5 MPa) at 260–300 °C and liquid feed weight-hourly space velocity in the range 2–8 h^{-1}. Due to the same method of preparation and activation (sulfidation) of the catalysts, the final properties were affected mainly by the differences in the nature of supports as well as their properties, such as specific surface area, pore size distribution or acidity. Most notably the dispersion of the active phase decreased in the following order $SiO_2 > Al_2O_3 > TiO_2$. As a result, the SiO_2-supported NiMo catalyst exhibited smaller extent of hydrogenation reactions and a larger extent of decarboxylation. On the other hand, the TiO_2-supported NiMo catalyst exhibited increased selectivity to hydrodeoxygenation products, plausible due to the larger active phase cluster size and broad pore size distribution. The results provide clear evidence that even with the conventional hydrotreating active phase, such as sulfided NiMo, the selectivity can be fine-tuned by support selection and modification.

1. Introduction

Deoxygenation of triglycerides is one of key processes making possible a convenient production of high quality automotive fuels components (sulfur-, oxygen- and aromatics-free). Various alternative routes for upgrading of triglycerides and related feedstocks, such as free fatty acids, into hydrocarbons have been reported in the literature [1–3]. Three most promising options include (i) catalytic cracking of triglycerides [4–11] under conditions similar to those of fluid catalytic cracking, (ii) decarboxylation using supported Pd catalysts [12–19] and (iii) hydrotreating using conventional hydrotreating catalysts, i.e. supported sulfides of Mo or W promoted by Ni or Co [20–32].

The advantage of catalytic cracking is that deoxygenation can be accomplished without hydrogen consumption. However, the process exhibits rather low selectivity towards diesel fuel components as gaseous and gasoline-range products are formed. The yields vary significantly depending on the catalyst type [4,7–9,11]. The highest yield of diesel cut products were obtained when using hierarchical zeolites (micro-mesoporous materials, such as ZSM-5–MCM-41) [8,33]. Moreover, due to the acid nature of cracking catalysts, cyclization and hydrogen transfer reactions resulting in formation of aromatics take place in addition to cracking and deoxygenation reactions. Consequently, the diesel fuel properties (cetane number, aromatics content) are worse as compared with hydrodeoxygenation products.

The alternative approach using noble metal catalysts, particularly palladium on carbon, is highly selective, as fatty acids undergo virtually exclusively decarboxylation [12]. Moreover, the reaction does not per se consume hydrogen [12], nonetheless, it has been demonstrated that hydrogen helps in preventing rapid catalyst deactivation by side reactions [14,17,19]. Hydrogen is also needed to saturate any double bonds in the fatty acid moieties to be deoxygenated in order to obtain deoxygenated product having good thermal and oxidation stability. From the industrial perspective point of view, long-term stability and activity of Pd/C catalysts for deoxygenation was not yet demonstrated hindering their widespread application. Recently, another alternative class of catalytic materials has attracted attention for deoxygenation of triglycerides, namely carbides, nitrides and phosphides of molybdenum or nickel [34–36]. These materials offer several advantages for processing of neat triglycerides as these catalysts are stable with time-on-stream [36] and co-feeding of sulfur-containing compounds, which is required for sulfided catalysts to maintain their activity, can be avoided. Since these catalysts are sulfur resistant, co-processing of refinery feeds with triglycerides is possible as well [36].

In contrast to the previous two alternatives, sulfided hydrotreating catalysts have been shown as active and selective catalysts and

* Corresponding author.
E-mail address: david.kubicka@vuanch.cz (D. Kubička).

0926-3373/$ – see front matter © 2013 Elsevier B.V. All rights reserved.
http://dx.doi.org/10.1016/j.apcatb.2013.01.012

have been also employed commercially [37,38]. While diesel fuel components are obtained selectively, the only by-products being water, carbon oxides and propane, even at total conversion, and the catalysts are well-known and widely used in the industry, there are several disadvantages to this approach. They include higher consumption of hydrogen than in decarboxylation or cracking [1], need of an external sulfur source to keep the sulfided catalyst in active state [30] and possible formation of sulfur species in the final product [39]. Generally, the formation of new sulfur-containing species is rather limited not threatening the diesel fuel specification limits and hydrogen-sulfide-containing hydrogen streams are readily available in conventional refineries. Hence, the most significant challenge, both from the environmental as well as economical point of view, is the high hydrogen consumption caused by the high oxygen content of triglycerides and fatty acids (ca. 11 wt.%).

The issue can be, in principal, tackled by varying the selectivity of the two main reaction pathways, namely hydrodeoxygenation (HDO) and decarboxylation (HDC). Assuming a model triglyceride consisting exclusively of C_{18} fatty acids moieties, then in HDO is oxygen eliminated as water and *n*-octadecane (*n*-C_{18}) is formed while in HDC oxygen is removed primarily as CO_2 and *n*-heptadecane (*n*-C_{17}) is formed. Looking at the different stoichiometric requirements for hydrogen consumption in the just described reaction pathways, it becomes obvious that hydrogen consumption could be reduced if one could steer the selectivity towards the HDC pathway. Another aspect that needs to be noted is that by favoring decarboxylation pathway, the yield of diesel fuel range products will be decreased (approximately by 5–6%), as there will be one carbon atom less in the final products than in the case of HDO reaction pathway.

The aim of the work is to investigate the effect of catalyst support on its deoxygenation performance, in particular on the selectivity towards HDO and HDC, respectively. Hence three NiMo catalysts having the same active phase composition were prepared using different industrially relevant supports (Al_2O_3, SiO_2, TiO_2). The deoxygenation performance focusing on deoxygenation products distribution was investigated under typical deoxygenation conditions reported previously [24,32] using rapeseed oil as model feedstock.

2. Experimental

2.1. Catalyst preparation and characterization

NiMo catalysts having the same loading of active components (Ni–3.3 wt.% and Mo–15 wt.%) and different support (Al_2O_3, SiO_2 and TiO_2) were prepared by incipient wetness. The commercial supports were crushed and the fraction 0.25–0.50 mm was used in catalyst preparation. Aqueous solutions of $Ni(NO_3)_2{\cdot}6H_2O$ and $(NH_4)_6Mo_7O_{24}{\cdot}4H_2O$ were used as the source of nickel and molybdenum, respectively. A two-step procedure was applied. At first the catalyst was impregnated with $(NH_4)_6Mo_7O_{24}{\cdot}4H_2O$ to contain 15 wt.% Mo and dried at 95–100 °C. Then it was calcined in an oven at 400 °C. Subsequently, the Mo-containing support was impregnated with $Ni(NO_3)_2{\cdot}6H_2O$ to contain 3.3 wt.% of Ni and dried again at 95–100 °C. Finally, the catalyst was calcined at 400 °C. The same procedure was used for all three supports.

The catalysts were characterized by several physico-chemical methods to assess their relevant catalytic properties. The methods included N_2 physisorption isotherm, DR UV–vis and FTIR spectroscopy, H_2 TPR and NH_3 TPD, and elemental composition (C, S). Nitrogen physisorption method was used to determine textural properties of catalysts (specific surface area and pore size distribution) using a Micromeritics ASAP 2020 volumetric instrument at–196 °C, for details see [40]. The BET surface area was evaluated using adsorption data in a relative pressure range from 0.05 to 0.25 and mesopore size distributions were calculated using BJH algorithm using Harkins–Jura equation calibrated to accurately determine the pore diameter and volume.

The UV–vis diffuse reflectance spectra of dehydrated samples were measured using Cintra 303 spectrometer (GBC Scientific Equipment, Australia) equipped with a Spectralon-coated integrating sphere using a Spectralon coated discs as a standard. The spectra were recorded in the range of the wavelength 190–850 nm. Before the spectra measurement the samples were dehydrated and oxidized in the glass apparatus under static oxygen atmosphere (15 kPa) in two steps: 120 °C for 30 min and 450 °C for 60 min and subsequently cooled down to 250 °C and evacuated for 30 min. After the evacuation the samples were transferred into the quartz optical cuvette 5 mm thick and sealed under vacuum. This procedure guaranteed complete dehydration and defined oxidation state of all $NiMoO_x$ particles on the catalyst surface. The obtained reflectance spectra were transformed into the dependencies of Kubelka–Munk function $F(R_\infty)$ on the wavenumber [41].

Redox behavior and dispersion of $NiMoO_x$ surface species was investigated by the temperature programmed reduction by hydrogen (H_2-TPR) using the AutoChem 2920 (Micromeritics, USA). A 100 mg sample in a quartz U-tube microreactor was oxidized in oxygen flow at 450 °C for 60 min prior the TPR measurement. The reduction was carried out from 50 °C to 1 050 °C with a temperature gradient of 10 °C/min in flow (25 ml/min) of reducing gas (5 vol% H_2 in Ar). The changes of hydrogen concentration were monitored by the TCD detector and simultaneously hydrogen consumption and water formation was also detected on a quadrupole mass spectrometer OmniStar™ GDS 300 (Pfeiffer vacuum, Germany).

Acidity of supported NiMoO catalysts was investigated by the temperature programmed desorption of ammonia (NH_3-TPD). NH_3-TPD experiments were carried out on the same instrument as H_2-TPR. Before each experiment a 100 mg of sample were pretreated in a flow of dry oxygen at 450 °C for 60 min and after that the sample was exposed to NH_3 (5 vol% NH_3 in He) at 75 °C for 30 min. The physically adsorbed ammonia was removed by purging with a helium flow for 30 min. Then the TPD was performed in He flow (25 ml/min) with a temperature gradient of 10 °C/min and the desorbed NH_3 was monitored by a TCD detector and by mass spectrometer which allow a monitoring other products of desorption as well.

2.2. Catalytic experiments

The catalytic experiments were carried out in an electrically-heated fixed bed reactor (inner diameter 17 mm) using rapeseed oil as a feedstock (food grade quality, without addition of sulfiding agent) in presence of hydrogen (3.5 MPa) at 260–300 °C. The sulfiding agent was not used to have a clear view on the effect of support only. The liquid feed weight-hourly space velocity was varied in the range 2–8 h^{-1}, while the hydrogen to liquid feed ratio was kept constant at 50 mol/mol. A wide range of LHSV was used in order to evaluate the selectivity changes over a wide range of conversions and degrees of deoxygenation. The conversion and degree of deoxygenation is defined in Eqs. (1) and (2), respectively:

$$\text{Conversion} = \frac{C_{TG_0} - C_{TG}}{C_{TG_0}} \times 100 \quad (1)$$

$$\text{Degree of deoxygenation} = \frac{C_{OX_0} - C_{OX}}{C_{OX_0}} \times 100 \quad (2)$$

where C_{TG_0} and C_{OX_0} are the concentration of triglycerides and oxygen, respectively, in the feedstock, and C_{TG} and C_{OX} are the concentration of triglycerides and oxygen in products.

Table 1
Basic physico-chemical properties of studied catalysts.

	BET (m^2/g)	S (wt.%)	C (wt.%)
$NiMo/SiO_2$	343 (524)[a]	15.6	5.6
$NiMo/Al_2O_3$	177 (198)[a]	9.8	5.9
$NiMo/TiO_2$	117 (203)[a]	7.1	5.5

[a] The number in parentheses gives the BET surface area of the support.

The NiMo catalysts (particle size 0.25–0.50 mm) were loaded in the reactor and were diluted with silicon carbide (particle size 0.1 mm) to improve the temperature profile along the catalyst bed. The profile was monitored by three adjustable thermocouples placed in a thermowell located in the axis of the reactor. The void space above the catalyst bed was filled with silicon carbide and in this part of the reactor the feed and hydrogen were preheated, mixed and distributed over the reactor cross-section. The catalyst was activated (sulfided) in situ prior to each experiment using dimethyldisulfide (DMDS) in isooctane. The sulfiding procedure lasted 10 hours including a dwell at 340 °C.

Several samples from each reaction condition were collected and analyzed by GC equipped with an on-column injection system and a flame ionization detector. Details of the analytical method were reported previously elsewhere [24,32].

3. Results and discussion

3.1. Catalyst characterization

The catalysts were prepared by incipient wetness impregnation to contain the same concentration of active components, i.e. 3.3 wt.% Ni and 15.0 wt.% Mo. The final catalysts differed in their specific surface area as shown in Table 1. The sulfur content of the catalysts, measured after reaction, exhibited a linear correlation with the catalyst specific surface area as it increased from 7.1 wt.% for $NiMo/TiO_2$ to 15.6 wt.% for $NiMo/SiO_2$ (Table 1). Since the metal content and preparation and pre-treatment methods were identical, it can be concluded that the dispersion of the active NiMo phase increased in the order $TiO_2 < Al_2O_3 < SiO_2$ which can also be associated with the available specific surface area that increased in the same order. At the same time, the content of carbon, reflecting the amount of carbonaceous deposits on the catalyst surface, was virtually the same for all three catalysts regardless their total specific surface area (Table 1). This indicates that the deactivation reactions proceeded approximately at the same rate. Moreover, TiO_2-supported catalyst exhibited a rather broad pore size distribution, while SiO_2 and Al_2O_3-supported catalysts showed a narrow and unimodal pore size distribution centered around 6 and 9 nm,

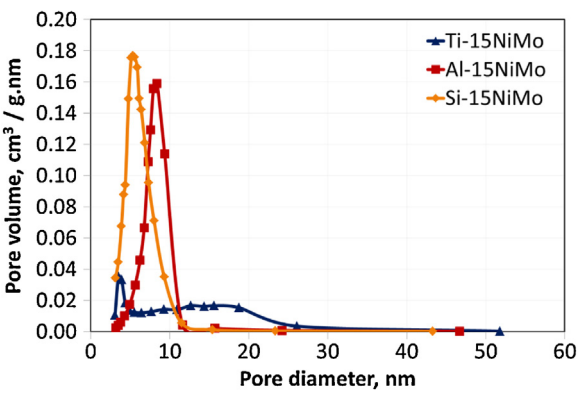

Fig. 1. Pore size distribution of the catalysts determined by BJH method.

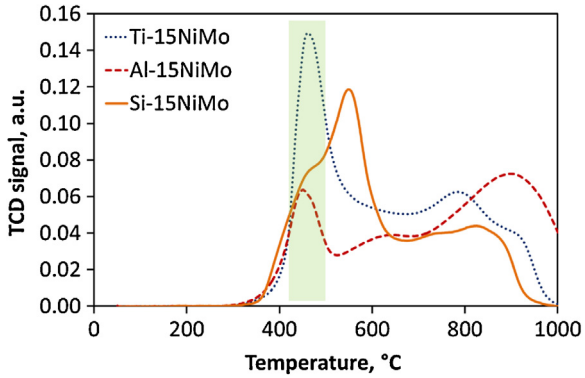

Fig. 2. Temperature programmed reduction (H_2-TPR) of catalysts. The shaded area (420–500 °C) shows the position of the first reduction peak.

respectively (Fig. 1). In all three cases the pore sizes are sufficient for triglycerides to enter them.

The catalysts exhibited different temperature programmed reduction profiles (H_2-TPR, Fig. 2) indicating that there were differences in the active phase-support interaction. The main reduction peak corresponding to the active phase reduction was located approximately between 350 and 600 °C (Fig. 2). As the active phase composition was identical, these differences could be explained by different strength of active phase-support interaction reflecting the support nature and active phase cluster size. The TiO_2-supported catalyst was the most easily reduced (reduction maximum at 460 °C) probably due to the largest active phase cluster size (as indicated by the lowest sulfur content in the sulfided catalyst) weakening the active phase-support interaction, whereas the SiO_2-supported catalyst showed a clear shift to higher reduction temperature (ca. 550 °C). It could be attributed to the smaller active phase cluster size (as indicated by the catalyst sulfur content, Table 1) and hence more intimate contact with the support (Fig. 2, Table 2). Finally, it was seen that alumina-supported catalyst was the most difficult to reduce suggesting a strong interaction of the intermediate clusters of active phase.

The UV–vis spectra of the catalysts did not exhibit any surprising features (Fig. 3). It could be seen that the nickel in tetrahedral coordination Ni(Td), typically recognizable by a band around 17000 cm^{-1}, was absent (Fig. 3, compare with [32]). A close inspection of the bands corresponding to nickel in octahedral coordination Ni(Oh) revealed though that there was an important difference in the intensity and hence in population of the Ni(Oh) species at ca. 22500 cm^{-1} in different catalysts (Fig. 3). While a very intense band was found in the case of SiO_2-supported catalyst, this band was absent in the case of alumina-supported catalyst and only a shoulder was visible (taking into account the shift of the edge) in the case of TiO_2-supported catalyst (Fig. 3). It might be speculated that this band could be connected with shift in H_2-TPR to higher reduction temperature and, in turn, with the differences in selectivity as discussed later. Obviously, further fundamental investigations are needed to prove or disprove this conclusion.

The measurements of temperature programmed desorption of ammonia demonstrated differences among the catalysts in the

Table 2
H_2-TPR and NH_3-TPD characteristic data.

	H_2-TPR		NH_3-TPD	
	H_2 consumption mmol	T_{max} (°C)	Desorbed NH_3 mmol	T_{max} (°C)
$NiMo/SiO_2$	3.0	549	108.1	160
$NiMo/Al_2O_3$	3.1	896	98.3	167
$NiMo/TiO_2$	3.7	461	54.1	195

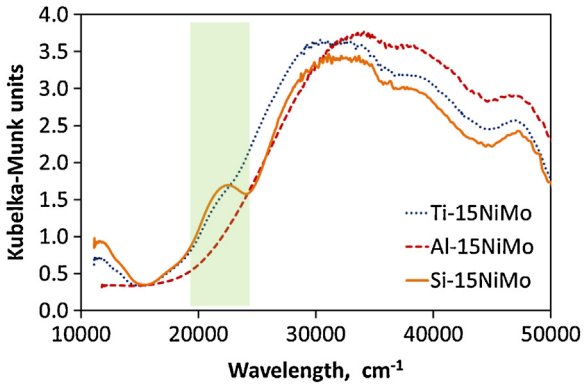

Fig. 3. UV–vis spectra of catalysts (in oxide form). The shade area shows the Ni(Oh) region exhibiting difference among the catalysts.

amount of acid sites interacting with ammonia as well as in their strength. The highest amount of acid sites contained the SiO_2-supported catalyst, which could be explained by the largest surface area and the best dispersion of the active phase resulting in high number of Lewis acid sites originating from dispersed $MoNiO_x$ phase and alternatively remaining silanols, as the desorption peak was at low temperature (ca. 160 °C, Fig. 4). A desorption peak at a similar position (desorption temperature) could be also seen in the remaining two catalysts. In contrast to SiO_2-supported catalyst, TiO_2- and Al_2O_3-supported catalysts had a second desorption peak with a maximum around 300 °C (Fig. 4). It was thus clear that there was another type of acid sites in these two catalysts and that these sites were stronger than the acid sites found in the SiO_2-supported catalyst. The population of these sites was the largest in the case of Al_2O_3-supported catalyst and it could be one of the reasons for stronger interaction between the active phase and support and consequently for the lower reducibility of the alumina-supported catalyst.

The catalyst characterization results showed rather convincingly that the SiO_2-supported NiMo catalyst exhibited, in spite of the same composition of the active phase and catalyst preparation and activation procedures, different properties than the other two catalysts (TiO_2- and Al_2O_3-NiMo supported catalysts). The above-discussed differences could be related to one common denominator, namely the interaction between the active phase and the support.

3.2. Catalytic experiments

Sulfided NiMo active phase supported on three different industrially relevant supports – Al_2O_3, SiO_2 and TiO_2 – had the ability to

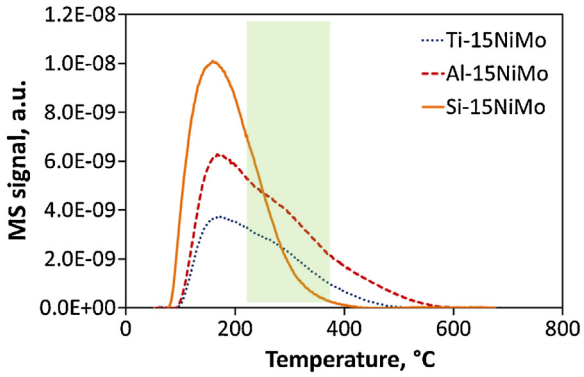

Fig. 4. Temperature-programmed desorption (TPD) of NH_3 of catalysts (in oxide form). The shaded area shows the second desorption peak of ammonia.

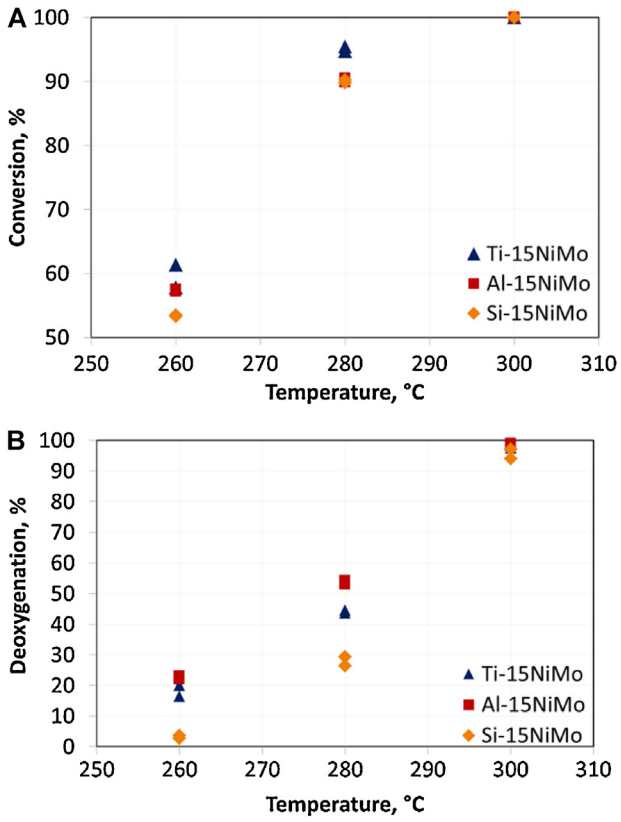

Fig. 5. Conversion, A, and deoxygenation, B of rapeseed oil as a function of reaction temperature (260–300 °C) at 4 h^{-1}, 3.5 MPa and 50 mol_{H_2}/mol_{feed}.

convert triglycerides completely into products at 300 °C (Fig. 5A). This is in line with previous reports [20,24,32]. With decreasing reaction temperature the conversion decreased and at 260 °C it was in the range 52–62% for all three catalysts (Fig. 5A). Despite the large conversion achieved, it can be clearly seen that the degree of deoxygenation (defined as reduction in oxygen content as compared to the feedstock, Eq. (2)) was significantly lower than conversion (Fig. 5B). The information about oxygen content was calculated from concentration of individual products determined by GC analysis of products. It can be observed that within the range of temperature ca. 250–300 °C, at WHSV of 4 h^{-1}, hydrogen pressure 3.5 MPa and hydrogen to feed ratio of 50 mol_{H2}/mol_{feed} the deoxygenation degree varied from 0 to 100%, i.e. from exclusive formation of oxygenated products to sole formation of hydrocarbons. It can be concluded that oxygenates are reaction intermediates.

This conclusion is valid in the entire experimental range, i.e. at 260–300 °C and 2–8 h^{-1} (Fig. 6) where yields of oxygenated products and hydrocarbons are plotted as a function of degree of deoxygenation. While the general trend in the dependence of the yields of oxygenated products on the degree of deoxygenation is an expected one, there are obvious differences among the studied supports. At the same degree of deoxygenation, the highest yield of hydrocarbons is obtained over SiO_2-supported catalyst and the lowest over TiO_2-supported catalyst (Fig. 6B). This is also reflected in the shift of the maximum on the yield curve of oxygenates towards higher deoxygenation degree from SiO_2 to TiO_2-supported catalyst (Fig. 6A). The difference among the supports stems from different relative reaction rates of hydrodeoxygenation (HDO) and decarboxylation (HDC) reactions over sulfided NiMo active phase supported on these supports. This can be clearly seen from analysis of yield curves of the main product groups that were denoted as oxygenated products, namely fatty acids, fatty alcohols and fatty esters.

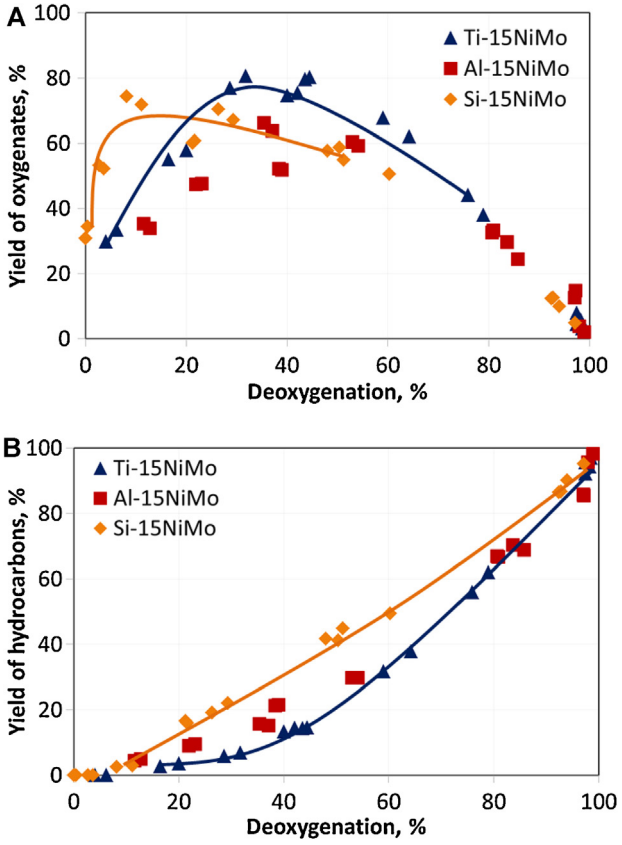

Fig. 6. Yields of the main product groups (oxygenated products (A) and hydrocarbons (B)) as a function of deoxygenation performance of the catalysts at 260–300 °C, 2–8 h^{-1}, 3.5 MPa and 50 mol_{H_2}/mol_{feed}.

The mutual interdependence (inter-conversion) of these products including formation of byproducts is schematically depicted in Fig. 7. Generally speaking, fatty acids originate from hydrogenolysis of triglycerides, fatty alcohols are products of reduction (hydrogenation) of carboxylic group in fatty acids and fatty esters are products of reaction between the former two groups of products. The yield curves support this claim as fatty acids can be seen as the primary products followed by fatty alcohols and fatty esters (Fig. 8A). The less pronounced yield curve of fatty alcohols (Fig. 8B) is a consequence of their higher reactivity in comparison with fatty acids or esters [42]. As a result, the concentration of fatty alcohols appears to be the rate-limiting step for the formation of fatty esters (Fig. 8C). The general scheme is in agreement with previous investigations [24].

An inspection of the Fig. 8 reveals that there is a significant difference among the supports. The high yield of fatty acids over SiO_2-supported NiMo catalyst in comparison with the remaining two supports (50 vs. ca. 20% at deoxygenation degree of ca. 25%, Fig. 8A) combined with the significantly lower yield of fatty esters

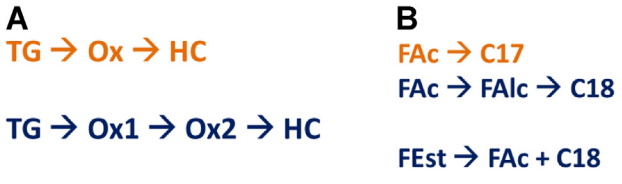

Fig. 7. Schematic representation of (A) triglycerides (TG) deoxygenation to oxygenated products (Ox) and hydrocarbons (HC) and of (B) fatty acid (FAc) intermediates deoxygenation to decarboxylation products (C17) or to fatty alcohols (FAlc) and hydrodeoxygenation products (C18). Fatty esters (FEst) deoxygenation is captured as well.

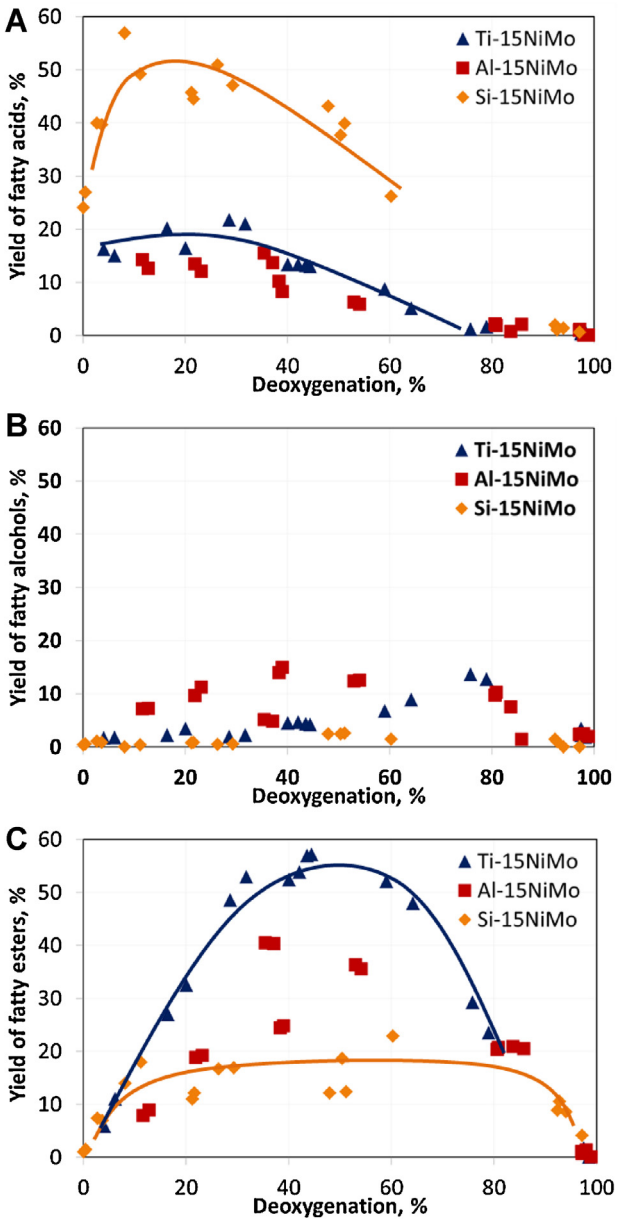

Fig. 8. Yields of fatty acid (A) fatty alcohols (B) and fatty esters (C) as a function of deoxygenation performance of the catalysts at 260–300 °C, 2–8 h^{-1}, 3.5 MPa and 50 mol_{H_2}/mol_{feed}.

(ca. 20% for SiO_2 vs. ca. 50% for TiO_2 at deoxygenation degree of ca. 25%, Fig. 8C) can be attributed to lack of fatty alcohols (Fig. 8B) in the product mixture. As the active phase and its composition is the same for all studied catalysts, it can be inferred that the differences are due to the involvement of the support, i.e. that the support affects the performance of the catalyst in other way than just influencing the active phase dispersion. The experimental data indicate that in the case of SiO_2-supported catalyst, fatty alcohols are not formed (Fig. 8B) rather than they are immediately consumed by deoxygenation. If it was the case, the fatty acids should have been consumed faster, as it is seen in the case of TiO_2 and Al_2O_3-supported catalysts (Fig. 8A). It can be thus concluded the catalyst hydrogenation performance in deoxygenation is affected by the support type. The performance of TiO_2 and Al_2O_3-supported catalysts is in this respect more similar to each other (Fig. 8), the main difference being the yield of fatty esters that is substantially lower in the case of Al_2O_3-supported catalyst (Fig. 8C). As the yield

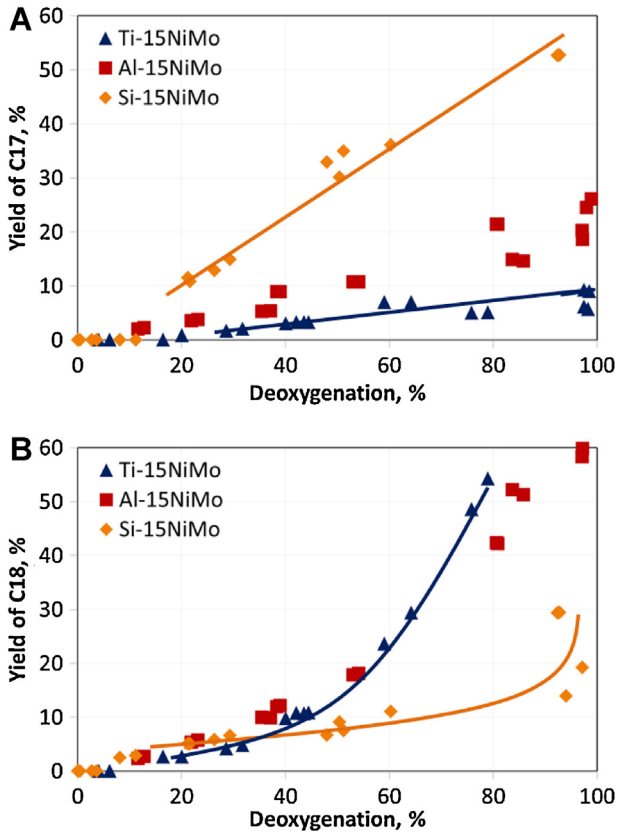

Fig. 9. Yields of *n*-heptadecane (A) and *n*-octadecane (B) as a function of deoxygenation performance of the catalysts at 260–300 °C, 2–8 h^{-1}, 3.5 MPa and 50 mol_{H_2}/mol_{feed}.

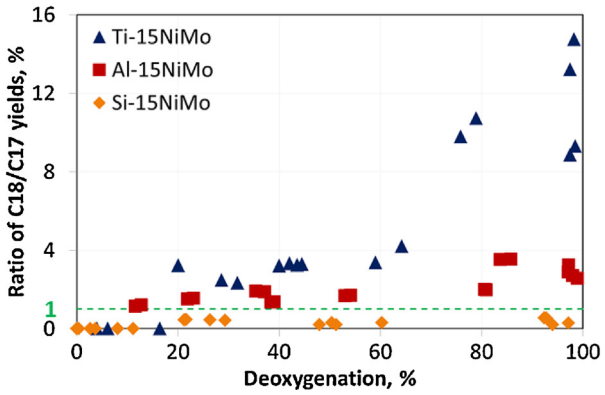

Fig. 10. Molar ratio of *n*-octadecane to *n*-heptadecane (C_{18}/C_{17}) as a function of deoxygenation performance of the catalysts at 260–300 °C, 2–8 h^{-1}, 3.5 MPa and 50 mol_{H_2}/mol_{feed}.

of fatty alcohols is at the same time slightly higher than in the case of TiO_2-supported catalyst, it can be suggested that the Al_2O_3 catalyst is more efficient in hydrogenation.

The observed differences in oxygenated products distribution are further propagated in the distribution of the ultimate deoxygenation products, hydrocarbons (Fig. 9). The SiO_2-supported NiMo catalyst yielded *n*-heptadecane as the main deoxygenation product, while Al_2O_3- and particularly TiO_2-supported catalysts afforded *n*-octadecane as the main deoxygenation product (Fig. 9). This means that over SiO_2-supported NiMo catalyst decarboxylation was preferred to hydrodeoxygenation. In contrast, over Al_2O_3 and above all TiO_2-supported NiMo catalysts hydrodeoxygenation was the predominant reaction pathway. The differences are summarized in Fig. 10 depicting the value of C_{18}/C_{17} ratio as a function of the overall deoxygenation degree. If equal to unity, there is the same extent of hydrodeoxygenation and decarboxylation. It can be seen that for SiO_2-supported catalyst the C_{18}/C_{17} ratio is less than one at complete deoxygenation, while over TiO_2-supported NiMo catalyst as high value as ten is achieved at complete deoxygenation (Fig. 10). With Al_2O_3-supported NiMo catalyst the final C_{18}/C_{17} ratio is about four (Fig. 10).

It is known that the preferred deoxygenation pathway can be related to catalyst composition. Alumina-supported Ni sulfided catalysts were shown to act virtually exclusively as decarboxylation catalysts whereas Mo sulfided catalysts exhibited a strong preference towards hydrodeoxygenation [24]. Variations in the yield of C_{17} and C_{18} hydrocarbons have been reported also for differently pretreated NiMo catalysts supported on Al_2O_3 [32]. It has been shown that with increasing content of NiO having tetrahedral coordination (result of high calcination temperature) the C_{18}/C_{17} ratio increased, i.e. that hydrodeoxygenation was preferred over decarboxylation [32].

As all the catalysts investigated here were pre-treated using the same procedure and the UV–vis spectra indicate that NiO is present only in octahedral coordination (Fig. 3), the noteworthy difference in C_{18}/C_{17} ratio (Fig. 10) among the investigated supports can be attributed to a role of the support. The SiO_2-supported NiMo catalyst affording mostly decarboxylation products, it can be inferred that it is a consequence of its different properties, namely higher dispersion giving rise to stronger active phase-support interaction. This can be observed not only in the shift in TPR profile to higher reduction temperature, but also plausibly by a specific Ni(Oh) band present in the UV–vis spectra at 22500 cm^{-1}. A plausible reason for the exceptional hydrodeoxygenation selectivity of the TiO_2-supported NiMo catalyst is not fully understood. The characterization results though indicate that the broad pore size distribution together with the largest active phase clusters among the tested catalyst might be the cause.

The differences in catalyst performance might originate not only from different interaction between the support and sulfide phase, but they can be plausibly related also to the differences in interaction between the oxides and the different supports. As seen from TPR, there is the formation of different types of metal oxide phase which could result in (after sulfiding) MoS_2 slabs having different stacking thus explaining the observed differences in deoxygenation selectivity. While the effects of promotion and structure (brim or edge sites, vacancies) of MoS_2 slabs and their influence on activity and selectivity of hydrotreating catalysts have been studied in great detail [43], there is still lack of knowledge regarding the relationship between deoxygenation activity/selectivity and catalyst structure although some theoretical and experimental attempts have been recently done [44].

4. Conclusions

Three different industrially important supports, SiO_2, TiO_2 and Al_2O_3, were used for preparation of NiMo catalysts to be used in deoxygenation of rapeseed oil. The catalysts were prepared using the same method and activation (sulfidation) procedure and had the same concentration of active components (3.3 wt.% Ni and 15.0 wt.% Mo). Due to the differences in the nature of supports as well as their properties, such as specific surface area, pore size distribution or acidity, the final properties differed as well. Most notably the dispersion of the active phase decreased in the following order $SiO_2 > Al_2O_3 > TiO_2$. Moreover, the different active phase cluster size and support nature were reflected in differences in active phase reducibility and in the character of Ni(Oh) species

that were the only NiO coordination type. These changes could be connected with the observed differences in catalyst selectivity as their overall activity was affected only to a lesser extent. The SiO_2-supported NiMo catalyst exhibited smaller extent of hydrogenation reactions and a larger extent of decarboxylation. As a result, *n*-heptadecane was the main product and at a given deoxygenation level less oxygenated products were yielded in comparison with the other two catalysts. On the other hand, the TiO_2-supported NiMo catalyst exhibited increased selectivity to hydrodeoxygenation products, plausible due to the larger active phase cluster size and broad pore size distribution. The results provide clear evidence that even with the conventional hydrotreating active phase, such as sulfided NiMo, the selectivity can be fine-tuned by support selection and modification.

Acknowledgements

The authors thank the Czech Science Foundation for financial support (Centre of Excellence–P106/12/G015). The project (P106/12/G015) is being carried out in the UniCRE centre (CZ.1.05/2.1.00/03.0071) in the Research Institute of Inorganic Chemistry.

References

[1] I. Kubičková, D. Kubička, Waste Biomass Valorization 1 (2010) 293.
[2] S. Lestari, P. Mäki-Arvela, J. Beltramini, G.Q. Max Lu, D.Yu. Murzin, ChemSusChem 2 (2009) 1109–1119.
[3] D. Kubička, I. Kubičková, J. Čejka, Catal. Rev. Sci. Eng. 55 (2013) 1–78.
[4] F.A. Twaiq, N.A.M. Zabidi, S. Bhatia, Industrial and Engineering Chemistry Research 38 (1999) 3230–3237.
[5] J.D. Adjaye, S.P.R. Katikaneni, N.N. Bakhshi, Fuel Processing Technology 48 (1996) 115–143.
[6] S.P.R. Katikaneni, J.D. Adjaye, N.N. Bakhshi, Canadian Journal of Chemical Engineering 73 (1995) 484–497.
[7] F.A. Twaiq, N.A.M. Zabidi, S. Bhatia, Microporous and Mesoporous Materials 64 (2003) 95–107.
[8] Y.-S. Ooi, R. Zakaria, A.R. Mohamed, S. Bhatia, Energy Fuels 19 (2005) 736–743.
[9] T. Danuthai, S. Jongpatiwut, T. Rirksomboon, S. Osman, D.E. Resasco, Applied Catalysis A: General 361 (2009) 99–105.
[10] T. Danuthai, S. Jongpatiwut, T. Rirksomboon, S. Osman, D.E. Resasco, Catalysis Letters 132 (2009) 197–204.
[11] T. Sooknoi, T. Danuthai, L.L. Lobban, R.G. Mallinson, D.E. Resasco, Journal of Catalysis 258 (2008) 199–209.
[12] I. Kubičková, M. Snåre, K. Eränen, P. Mäki-Arvela, D.Yu. Murzin, Catalysis Today 106 (2005) 197–200.
[13] I. Simakova, O. Simakova, P. Mäki-Arvela, A. Simakov, M. Estrada, D.Yu. Murzin, Applied Catalysis A: General 355 (2009) 100–108.
[14] P.T. Do, M. Chiappero, L.L. Lobban, D.E. Resasco, Catalysis Letters 130 (2009) 9–18.
[15] M. Snåre, I. Kubičková, P. Mäki-Arvela, K. Eränen, D.Yu. Murzin, Industrial and Engineering Chemistry Research 45 (2006) 5708–5715.
[16] P. Mäki-Arvela, I. Kubičková, M. Snåre, K. Eränen, D.Yu. Murzin, Energy Fuels 21 (2007) 30–41.
[17] B. Rozmyslowicz, P. Mäki-Arvela, A. Tokarev, A.-R. Leino, K. Eränen, D.Yu Murzin, Industrial and Engineering Chemistry Research 51 (2012) 8922–8927.
[18] L. Boda, G. Onyestyák, H. Solt, F. Lónyi, J. Valyon, A. Thernesz, Applied Catalysis A: General 374 (2010) 158–169.
[19] J.G. Immer, M.J. Kelly, H.H. Lamb, Applied Catalysis A: General 375 (2010) 134–139.
[20] B. Donnis, R.G. Egeberg, P. Blom, K.G. Knudsen, Topics in Catalysis 52 (2009) 229–240.
[21] G.N.d. Rocha Filho, D. Brodzki, G. Djega-Mariadassou, Fuel 72 (1993) 543–549.
[22] J. Gusmão, D. Brodzki, G. Djega-Mariadassou, R. Frety, Catalysis Today 5 (1989) 533–544.
[23] E. Laurent, B. Delmon, Applied Catalysis 109 (1994) 77–96.
[24] D. Kubička, L. Kaluža, Applied Catalysis A: General 372 (2010) 199–208.
[25] G.W. Huber, P. O'Connor, A. Corma, Applied Catalysis A: General 329 (2007) 120–129.
[26] D. Kubička, Collection of Czechoslovak Chemical Communications 73 (2008) 1015–1044.
[27] S. Bezergianni, A. Dimitriadis, A. Kalogianni, P. Pilavachi, Bioresource Technology 101 (2010) 6651.
[28] S. Bezergianni, A. Dimitriadis, T. Sfetsas, A. Kalogianni, Bioresource Technology 101 (2010) 7658.
[29] D. Kubička, M. Bejblová, J. Vlk, Topics in Catalysis 53 (2010) 168.
[30] D. Kubička, J. Horáček, Applied Catalysis A: General 394 (2011) 9.
[31] J. Mikulec, J. Cvengroš, L. Joríková, M. Banič, A. Kleinová, Chemical Engineering Transactions 18 (2009) 475.
[32] P. Priecel, D. Kubička, L. Čapek, Z. Bastl, P. Ryšánek, Applied Catalysis A: General 397 (2011) 127.
[33] F.A. Twaiq, A.R. Mohamad, S.P. Bhatia, Fuel Processing Technology 85 (2004) 1283.
[34] J. Monnier, H. Sulimma, A. Dalay, G. Caravaggio, Applied Catalysis A: General 382 (2010) 176.
[35] Y. Yang, C. Ochoa-Hernández, V.A.P. O'Shea, J.M. Coronado, D.P. Serrano, American Chemical Society Catalysis 2 (2012) 592.
[36] L.A. Sousa, J.L. Zotin, V. Teixeira da Silva, Applied Catalysis A: General 449 (2012) 105.
[37] Neste Oil, http://www.nesteoil.com/default.asp?path=1,41,11991,12243,13565, 2012 (accessed October, 2012).
[38] UOP, www.uop.com, UOP/ENI Ecofining Process.pdf, 2012 (accessed October 2012).
[39] T.-R. Viljava, E.R.M. Saari, A.O.I. Krause, Applied Catalysis A: General 209 (2001) 33.
[40] A. Zukal, H. Šiklová, J. Čejka, Langmuir 24 (2008) 9837.
[41] P. Kubelka, F. Munk, Zeitschrift Technical Physics 12 (1931) 593.
[42] E. Furimsky, Applied Catalysis A: General 199 147 (2000).
[43] A. Stanislaus, A. Marafi, M.S. Rana, Catalysis Today 153 (2010) 1.
[44] M. Ruinart de Brimont, C. Dupont, A. Daudin, C. Geantet, P. Raybaud, Journal of Catalysis 286 (2012) 153.